JCTC Journal of Chemical Theory and Computation

Article

pubs.acs.org/JCTC

Interfacial States in Donor−Acceptor Organic Heterojunctions: Computational Insights into Thiophene-Oligomer/Fullerene Junctions

Kakali Sen,[†] Rachel Crespo-Otero,[†] Oliver Weingart,[‡] Walter Thiel,[†] and Mario Barbatti*,[†]

[†]Max-Planck-Institut für Kohlenforschung, Kaiser-Wilhelm-Platz 1, D-45470 Mülheim, Germany

[‡]Institut für Theoretische Chemie und Computerchemie, Heinrich-Heine-Universität Düsseldorf, Universitätsstrasse 1, D-40225 Düsseldorf, Germany

Supporting Information

ABSTRACT: Donor−acceptor heterojunctions composed of thiophene oligomers and C_{60} fullerene were investigated with computational methods. Benchmark calculations were performed with time-dependent density functional theory. The effects of varying the density functional, the number of oligomers, the intermolecular distance, the medium polarization, and the chemical functionalization of the monomers were analyzed. The results are presented in terms of diagrams where the electronic states are classified as locally excited states, charge-transfer states, and delocalized states. The effects of each option for computational simulations of realistic heterojunctions employed in photovoltaic devices are evaluated and discussed.

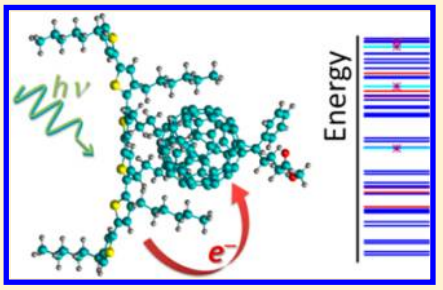

I. INTRODUCTION

In recent years, organic heterojunctions have been extensively explored for photodevices. They are promising materials because of their potential low cost and plastic properties.[1−7] The photophysics of an organic heterojunction composed of blended electron-donor and electron-acceptor materials is based on the photoexcitation of the donor, which is also a chromophore, followed by an electron-charge transfer to the acceptor. For an efficient photodevice, this process occurs, ideally, with small rates of charge-recombination and of photochemical or photophysical quenching. Many groups around the world have proposed and tested a large number of different heterojunctions.[4,7] In spite of all this effort, the efficiency of organic solar cells is still low in comparison to other classes of solar cells, barely reaching 10%.[8]

The search for new and more efficient junctions goes through the cumbersome process of designing new molecular complexes, heuristically improving certain properties of the previous generation of complexes. In this sense, computational chemistry may be a valuable tool, as it can be used to prescreen large numbers of different molecular complexes without the costs and difficulties of laboratory synthesis. In spite of the success of phenomenological models, which rely on empirical parametrization,[6] the potential of computational chemistry in this particular field has, however, been underused. The main reasons are, first, the difficulties of translating the usually computed quantities into relevant information for experimentalists; second, the difficulty of establishing standard computational procedures to be applied semiautomatically for new complexes; and, third, the increase of computational costs associated with the relatively large molecules forming heterojunctions.

A series of computational studies of organic heterojunctions have appeared recently. Microelectrostatic analysis, semiempirical methods, density functional theory (DFT), and many-body Green's function approximations have been used to assess the excited-state properties of organic heterojunctions.[9−22] In some of these works, excitations are characterized in terms of single particle models,[10,16] where the excited states are approximated by single electron transitions between two orbitals. This is certainly a very strong restriction and can thus only be regarded as a first qualitative approach. In most computational studies, excitations are accessed via time-dependent (TD) DFT.[13−15,18,19,21,22] Although a TDDFT treatment is more appropriate to approach the problem, many methodological issues are still of concern and may strongly affect the quality of the results. These issues are either related to the computational level (functional, basis sets, limitations of TDDFT to deal with double excitations) or to the modeling (use of short oligomers for polymers, neglecting large inactive functional groups and environmental effects). Many of these issues have been discussed in previous works and a working knowledge has been established. For instance, it is quite evident that pure and hybrid functionals will not adequately describe the charge-transfer (CT) states at the heterojunctions; and most of recent works have been using range-separated functionals to deal with this issue.[14,18,19]

Received: September 28, 2012
Published: November 21, 2012

In the present work, we conduct an investigation of the main methodological issues affecting the quality of the computational results. This is done systematically so as to provide a useful benchmark for future work in the field. Our investigations are focused on the description of the electronically excited states of thiophene-oligomer/fullerene interfaces (Figure 1), which are

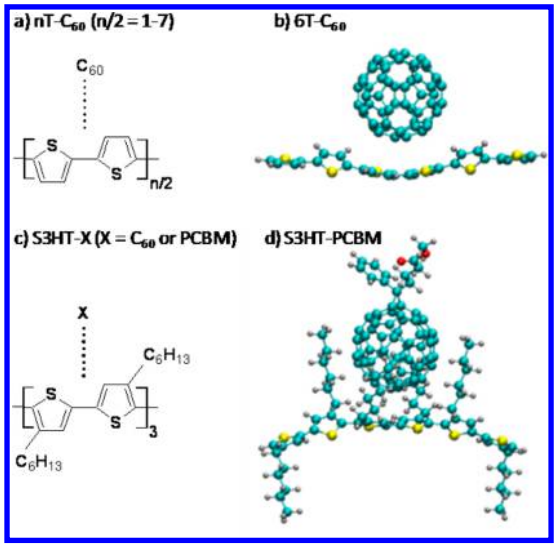

Figure 1. (a) Geometric scheme of the nT-C_{60} complexes. (b) Optimized geometry of the 6T-C_{60} complex (n = 6). (c) Geometric scheme of the S3HT-X (X = C_{60} or PCBM) complexes. (d) Optimized geometry of the S3HT-PCBM complex obtained at the ωB97X-D/6-31G(d) level.

the basis for several of the most efficient organic heterojunctions. We have studied donor chains (nT) with up to 14 thiophene monomers complexed with fullerene (C_{60}), a very efficient electron acceptor. In addition, the effect of functionalization of 6T into sexi(3-hexylthiophene) (S3HT)—a model for the well-known poly(3-hexylthiophene) (P3HT)[23]—and of C_{60} into [6,6]-phenyl-C_{61}-butyric acid methyl ester (PCBM)[24] has also been investigated.

We will show that, although TDDFT may provide a qualitatively adequate description of the electronic structure of D−A heterojunctions, the quantitative results still depend too much on methodological aspects and on the level of treatment of environmental effects. These are important limitations for a full understanding of these systems.

II. COMPUTATIONAL DETAILS

Ground-state geometries of the monomers and complexes were optimized with DFT using the ωB97X-D functional.[25] Cartesian coordinates are provided in the Supporting Information. Excited-states were computed with TDDFT mostly using this functional. Complementary calculations were also done using B3LYP,[26,27] PBE0,[28] LC-BLYP,[29−31] CAM-B3LYP,[32] M06-2X,[33] and M06-HF[34] functionals; these functionals are characterized in the Supporting Information, Table SI-1. The 6-31G(d) basis set[35] was adopted for most of the computations. Supplementary calculations used the 6-311G(df,2p) basis set. All TDDFT calculations were performed with Gaussian 09.[36]

State classification was performed with a variation of the method that we have described in ref 37. The molecular system is split in two units, A and B (later in the paper, A will be associated with the acceptor and B with the donor). Using a Mulliken partition, the integrated electron density in molecular orbital k of unit A is

$$\rho_A^k = \sum_{\mu\in A,\nu\in A} c_{\mu k}c_{\nu k}S_{\mu\nu} + \sum_{\mu\in A,\nu\in B} c_{\mu k}c_{\nu k}S_{\mu\nu} \quad (1)$$

where $S_{\mu\nu} \equiv \langle\varphi_\mu|\varphi_\nu\rangle$ is the overlap integral between basis functions φ_μ and φ_ν. $c_{\mu k}$ denotes the molecular orbital coefficients for orbital k and basis function φ_μ. Considering an electronic transition from orbital i to j, the quantity $\rho_A^j + \rho_A^i$ indicates how localized in A the transition is, while the quantity $\rho_A^j - \rho_A^i$ is a measure of the charge transfer between A and B. To take into account the multielectronic character of the excitation, we suppose that an electronic state I can be represented as a singly excited configuration-interaction wave function.[38] Then, the quantities

$$\Sigma P_A^I = \sum_{i\to j} \sigma_{ij}(C_{i\to j}^I)^2(\rho_A^j + \rho_A^i) \quad (2)$$

$$\Delta P_A^I = \sum_{i\to j} \sigma_{ij}(C_{i\to j}^I)^2(\rho_A^j - \rho_A^i) \quad (3)$$

for unit A are computed. In these equations, $C_{i\to j}^I$ is the coefficient corresponding to an excitation from orbital i to j. In TDDFT, σ_{ij} is 1 for $i < j$ and −1 for $i > j$. Practical hints about the state classification are given in section II of the Supporting Information.

Using eqs 2 and 3, state I is classified as local excitation in A [LOC(A)] if $\Sigma P_A^I \geq 1.5$ or in B [LOC(B)] if $\Sigma P_A^I \leq 0.5$; as an electron charge transfer from A to B [CT A→B] if $\Sigma P_A^I \leq -0.5$ or from B to A [CT B→A] if $\Sigma P_A^I \geq 0.5$; and as a delocalized excitation over A and B (DELOC) otherwise. This classification criterion is illustrated in Figure 2. The gray regions correspond

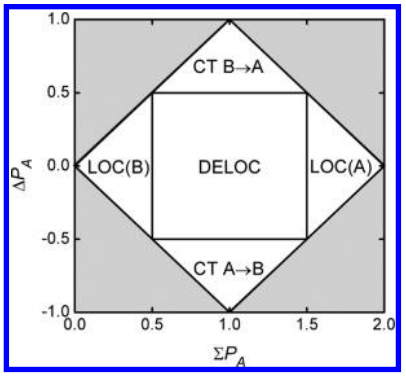

Figure 2. State classification in terms of delocalized (DELOC), charge transfer (CT), and localized (LOC) states.

to forbidden regions with negative electronic density in A or B, supposing that the orbitals are entirely localized either in A or B. A related method for state classification has been recently applied to heterojunctions in ref 20.

The absorption spectra of C_{60} and of 6T in the gas phase were computed with the nuclear ensemble approximation[37,39] using the Newton-X program.[40,41] DFT/MRCI[42] calculations based on Kohn−Sham orbitals computed with Turbomole[43] were performed with the BHLYP functional.[44] The SV(P) basis set[45] was adopted in these calculations. Auxiliary basis functions for the resolution-of-identity approximation of two-electron integrals were taken from the Turbomole library.[43,46] In the

dx.doi.org/10.1021/ct300844y | J. Chem. Theory Comput. 2013, 9, 533−542

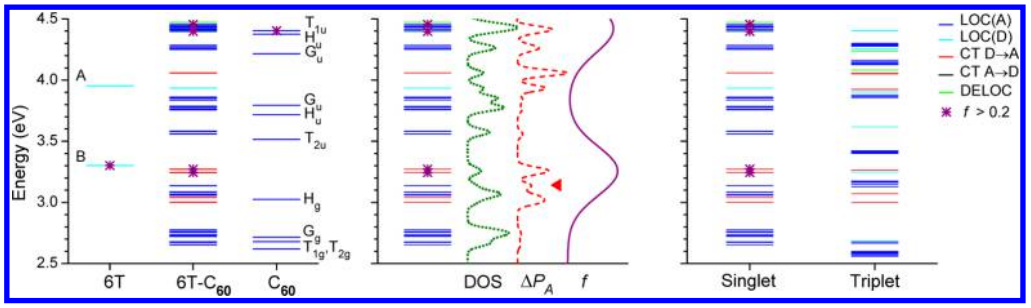

Figure 3. Left: Singlet electronic states of 6T (C_2 symmetry), C_{60} (I_h symmetry), and of the 6T-C_{60} complex. Middle: Singlet electronic states of 6T-C_{60}, density of states (DOS), charge transfer amount (ΔP_A), and oscillator strength (f). The DOS, ΔP_A, and f were convoluted over all states using Gaussian line shapes. The triangle near ΔP_A indicates the classical estimate for the energy of the lowest charge-transfer state. Right: singlet and triplet electronic states of the 6T-C_{60} complex. All calculations were performed at the TD-ωB97X-D/6-31G(d) level.

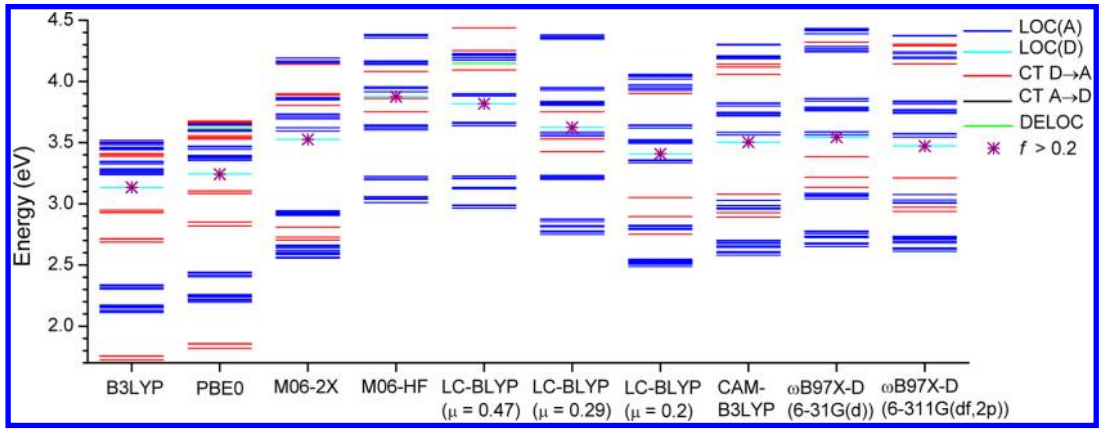

Figure 4. Singlet excited states of the 4T-C_{60} complex computed with TDDFT and different functionals. Unless indicated otherwise, the 6-31G(d) basis set was used. The ground state geometry was optimized at the ωB97X-D/6-31G(d) level. The star indicates the bright states (oscillator strength larger than 0.2).

DFT/MRCI method, the MRCI formalism is modified by incorporating five universal empirical parameters to alleviate problems with the double counting of dynamic electron correlation. Since dynamic correlation is conceptually incorporated through the DFT treatment, DFT/MRCI requires only rather few reference configurations and rather small CI spaces. An energy-based selection criterion is iteratively applied to disregard all configurations with energies above a certain configuration selection threshold (1.0 hartree). In this work, the initial reference configurations were generated by exciting up to two electrons out of 16 electrons in 16 active orbitals.

III. RESULTS AND DISCUSSIONS

Monomeric and Interfacial States. We start our discussion by describing the electronically excited states of the 6T and C_{60} monomers and of the 6T-C_{60} complex in the gas phase. The level diagram in Figure 3-left illustrates the vertical excitation energies computed at the ground-state geometry of each molecule. The color code in this figure, as well as in the remaining figures of this paper, indicates the character of each state. It should be noted that the levels in these diagrams are the energies of electronic states within a multielectronic approach and not orbital energies. The star symbol indicates states with oscillator strength larger than 0.2. All information provided in the graphs is given as tables in the Supporting Information.

6T has C_2 symmetry in the ground state. The first singlet excited state, 1^1B, is a bright state, while the second, 2^1A, is dark (Figure 3-left). C_{60} belongs to the I_h point group. The first singlet excited states are dark states belonging to the T_{1g}, T_{2g}, and G_g representations. Throughout this paper, they will be referred as the first band of C_{60}. The dark 1^1H_g state comes next in energy (second band). It is followed by a group of three other dark states, 1^1T_{2u}, 1^1H_u, and 1^1G_u (third band). The fourth band contains the dark 2^1G_u and 2^1H_u states and the first bright 1^1T_{1u} state.

The stacked 6T-C_{60} complex investigated here has C_2 symmetry. Most of the excited states keep a good resemblance to the states of the monomers (Figure 3-left). The high degeneracy of the C_{60} states is broken giving rise to broad and dense bands. The bright state of 6T is slightly stabilized and acquires a strong CT D→A character (the apparent contradiction of having a bright CT state is discussed later). A series of CT D→A states is spread through the spectrum, the lowest one at 3.00 eV. No CT A→D state was observed below 4.5 eV. Two delocalized states lie in the highest band.

The density of states (DOS), charge-transfer amount (ΔP_A), and oscillator strength (f) are shown together with the energy levels of the 6T-C_{60} complex in Figure 3-middle. They are given as Gaussian-convoluted values over all computed states. For DOS and ΔP_A, the width of the Gaussian functions was 0.05 eV. For f, it was 0.4 eV, the typical vibrational broadening of the bright band. These curves help to understand the photophysics of the D−A complexes by introducing new information not apparent in the energy level diagrams. For instance, note how the LOC(D) state at 3.93 eV in the ΔP_A curve has a large amount of electron charge transfer character.

dx.doi.org/10.1021/ct300844y | J. Chem. Theory Comput. 2013, 9, 533−542

Singlet and triplet excited states of the 6T-C_{60} complex are shown in Figure 3-right. As usual, the triplet bands are at lower energy than the corresponding singlet bands. The charge transfer states, however, have similar energies in the singlet and triplet manifolds because of the small exchange interactions between the two monomers. This is expected to be a common feature in D−A complexes.

Effect of the Computational Level. *Density Functional Dependence.* In TDDFT, the major factor affecting the results is the density functional. Figure 4 shows the electronic states of the 4T-C_{60} complex in the ground-state geometry computed with several functionals. These functionals were selected to give an overview over a broad range of Hartree−Fock (HF) exchange contributions (see Supporting Information, Table SI-1).

Apart from the D−A distance, the computed ground-state geometries do not depend much on the functional, as confirmed by tests using LC-BLYP, B3LYP, and ωB97X-D. The main difference arises from the dispersion correction (included in ωB97X-D) since the complexes may not be stable without this correction. If the D−A distance is fixed during the optimization, the geometry of the monomers is very similar for all functionals investigated.

The vertical excitation energies show strong dependence on the functional (Figure 4). The CT states are especially affected. It is well-known[47] that the erroneous long-range behavior of the exchange part of the functional in B3LYP, PBE0, and, to a lesser extent, M06-2X causes an underestimation of the CT energies. The lowest CT states computed with these functionals are located either much below the first C_{60} band (B3LYP and PBE0) or between the first and second C_{60} bands (M06-2X). According to M06-HF (with 100% HF exchange) and the range-separated functionals, the lowest CT states should be always above the first band.

The CT energies are quite dependent on the range-definition parameter μ of the range-separated functionals. This point is illustrated for LC-BLYP in Figure 4. The default value adopted in Gaussian 09, μ = 0.47 a_0^{-1}, leads to a clear overestimation of the CT energies, located around the fourth C_{60} band. Reparameterization of this functional based on empirical data[48] indicates that better results should be obtained for μ = 0.29 a_0^{-1}. A similar value is adopted by the GAMESS program[49] (μ = 0.33 a_0^{-1}, see also ref 50). With μ = 0.29 a_0^{-1}, the CT states are below the third C_{60} band. Nonempirical reparameterization[18] of the LC-BLYP functional leads to an even smaller value for μ (0.2 a_0^{-1}). In this case, the CT states are distributed around the second band, similarly to CAM-B3LYP results. ωB97X-D distributes the CT states between the second and third C_{60} bands, an intermediary result between M06-HF and LC-BLYP(0.29) on one hand and LC-BLYP(0.20)/CAM-B3LYP on the other.

The first bright state, localized in 4T, can be as low as 3.13 eV with B3LYP or as high as 3.88 eV with M06-HF (Figure 4). Among the hybrid functionals, the increase of HF exchange destabilizes this state. Among the range-separated functionals, the decrease of μ stabilizes it. The bright state lies within 0.12 eV when computed with LC-BLYP (0.2 or 0.29), CAM-B3LYP, and ωB97X-D. In the case of CAM-B3LYP and ωB97X-D, the bright state is right below the third C_{60} band. This is also true for M06-2X, which is especially suitable to predict this type of state.

We expect that the behavior of the different functionals is similar for the excited states of larger complexes (n > 4). This is confirmed by tests with 6T-C_{60} showing that the excitation energies of C_{60} localized states are still overestimated with range-separated functionals, whereas those of CT-states are underestimated with non-range-separated functionals.

The basis set has a smaller impact on the excitation energies than the functional, as shown in Figure 4 for 4T-C_{60} computed with TD-ωB97X-D using the 6-31G(d) and the 6-311G(df,2p) basis sets. With the triple-ζ basis set, the bright local excitation in 4T is stabilized by 0.07 eV and the C_{60} localized electronic states are stabilized by only 0.03 eV on average (maximum stabilization 0.05 eV). The CT D→A states are more affected. With the triple-ζ basis, they are stabilized by 0.2 eV on average, with maximum stabilization of 0.25 eV. Consequently, a CT D→A state becomes the lowest state in the second band.

Multiple Excitations. In the simulation of complexes, there is always the possibility of an unbalanced treatment of the monomers, in the sense that local excitations are reproduced with different accuracy in each monomer. This would endanger the computational description of the D−A photophysics at TDDFT level, which depends on the accurate prediction of the relative energies of local and CT states. To verify this point, we have computed the vertical electronic states of isolated 6T and C_{60} monomers using the DFT/MRCI method. (Unfortunately, it was not possible to treat the full complex at this level.) DFT/MRCI can provide accurate results.[51] It also includes multireference and multiple excitation contributions to the states, features missing in TDDFT. The comparison between the TD-ωB97X-D/6-31G(d) and DFT/MRCI/SV(P) results is shown in Figure 5. In the region below 4 eV (DFT/MRCI scale), TDDFT energies of both molecules are systematically larger than DFT/MRCI energies by approximately the same amount (~0.5 eV), indicating that TDDFT treats the two molecules in a balanced manner (exceptions are discussed below).

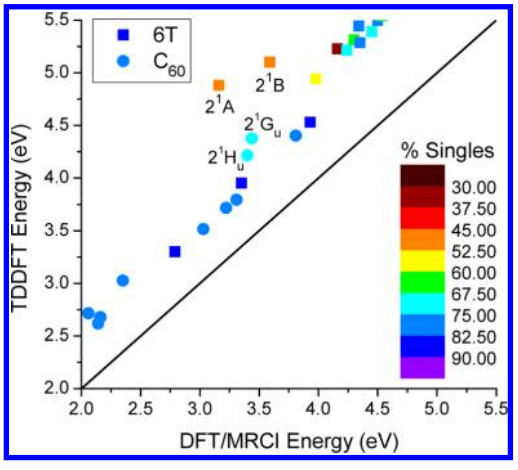

Figure 5. Excited-state energies of 6T and C_{60} computed with TD-ωB97X-D/6-31G(d) in comparison to the energies computed with the DFT/MRCI/SV(P) method. The color code indicates the total fraction of single excitations for each state.

The lack of double excitations in the linear-response TDDFT is another problem of concern.[52] For each state in Figure 5, the total weight of single excitations, as given by the DFT/MRCI approach, is also indicated. Most of the states have more than 75% of single excitations. According to DFT/MRCI, the lowest multiply excited states of 6T lie at 3.16 and 3.59 eV, while the lowest bright state lies at 2.79 eV. It is fortunate that the

dx.doi.org/10.1021/ct300844y | J. Chem. Theory Comput. 2013, 9, 533−542

multiply excited states of 6T are above the bright state; if this were not the case, the description of 6T-C_{60} photophysics based on TDDFT would not be adequate.

As we have already discussed, up to 4 eV (DFT/MRCI scale), the deviation between TDDFT and DFT/MRCI is about 0.5 eV for both molecules. There are four exceptions in this region: the 2^1G_u and 2^1H_u states of C_{60} (deviations 0.8 and 0.9 eV) and the 2^1A and 2^1B states of 6T (deviations 1.7 and 1.5 eV). These four states are characterized by a small weight of single excitations, ~70% in the case of two C_{60} states, and ~50% in the case of the two 6T states, which indicates an inverse correlation between the size of the deviation and the amount of single excitations. However, above 4 eV, the deviations between the two methods increase to about 1 eV, independently of the amount of single excitations.

Vibronic Spectrum Predictions. The comparison between TDDFT results and experiments can be aided by computing the vibronic broadening of the absorption spectrum. Figure 6 shows the simulated spectrum of 6T and C_{60} using the nuclear ensemble approximation, which allows us to predict the bandwidth and intensity of bright and dark vibronic bands.[37] The parameters for the spectrum simulation are given in the Supporting Information, Table SI-2.

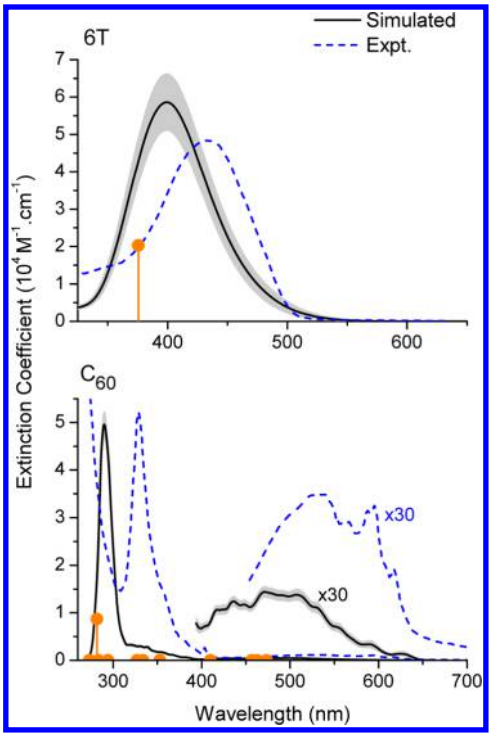

Figure 6. Absorption spectra of 6T and C_{60} computed at TD-ωB97X-D/6-31G(d) level. The shaded gray areas indicate the error bar in the numerical integration of the spectrum. The dots indicate the vertical excitation energies and oscillator strengths computed at the same level. Experimental data for C_{60} in *n*-hexane[53] and for 6T in benzene.[54]

In the case of 6T (Figure 6-top), the simulation in the gas phase shows a single band centered at 399 nm (3.11 eV). This band, associated with the 1^1B state, is blue-shifted in relation to the experimental band measured in benzene[54] by 0.2 eV. The vertical excitation (shown as a dot in Figure 6-top) is blue-shifted in relation to the simulated band maximum by 0.14 eV (see also Table 1).

Table 1. Comparison of the Computational Predictions for Vertical Excitations and Band Maxima with the Experimental Band Maxima

	TD-ωB97X-D		expt.
	vert. exc. (eV)	band max. (eV)	band max. (eV)
6T	3.25	3.11	2.9,[b] 2.3–2.4[c]
C_{60} (1^1T_{1g},1^1T_{2g},1^1G_g)[a]	2.62, 2.68, 2.72	2.60	2.31[d]
C_{60} (1^1T_{1u})	4.40	4.28	3.8,[d] 3.4[e]
S3HT-PCBM	3.51	2.6[f]	2.2–3.1,[g] 2.6[h]

[a]Dark band. [b]Benzene solution, ref 54. [c]Film, refs 56–58. [d]*n*-hexane solution. Data from ref 53 as assigned in ref 59. [e]Film, ref 60. [f]Corrected value. See text. [g]Depending on the fabrication method and PCBM amount (see Supporting Information), refs 24,61,62. [h]Film (spin-coated, 50 wt.% PCBM), ref 62.

The predicted extinction coefficient for 6T (Figure 6-top) is larger than the experimental result. In the nuclear ensemble approximation, the value of the extinction coefficient has a degree of arbitrariness because of the free parameter δ (see Supporting Information, Table SI-2). A basic criterion to fix δ is to choose its value as the largest one that does not interfere with the bandwidth. The simulation of a number of different molecules has indicated that a value of 0.05 eV,[37,39] which is much narrower than the bandwidth, leads to a good prediction of the extinction coefficient. In the case of 6T, the δ value obtained in this manner is 0.3 eV, much higher than in other cases. As discussed in refs 37,55 such a large value indicates that 6T leaves the Franck–Condon region within few femtoseconds after the photoexcitation.[37,55]

In the case of C_{60} (Figure 6-bottom), the simulated spectrum in the gas phase features a bright band at 290 nm (4.28 eV) associated with the 1^1T_{1u} state, a weak shoulder at ~350 nm (3.54 eV) associated with the 1^1T_{2u}, 1^1G_u, and 1^1H_u states, and a broad but dark band centered at 477 nm (2.60 eV) associated with the 1^1T_{1g}, 1^1T_{2g}, and 1^1G_g states. The maximum of the dark band is blue-shifted by 0.29 eV compared to experiments in *n*-hexane[53] (Table 1). The bright band, however, is blue-shifted by 0.48 eV in comparison to the same experimental data. The shift of this band is a particular drawback of the tested range-separated functionals. The prediction of the first bright band of C_{60} is more accurate with conventional functionals and semiempirical methods.[59,63,64] The 1^1T_{1u} vertical excitation is blue-shifted by 0.12 eV in relation to the simulated band maximum.

The simulated extinction coefficient of the bright band of C_{60} is in excellent agreement with the experiment. The extinction coefficient of the dark band, however, is somewhat smaller than the experimental value. This is a consequence of the large blue shift of the bright state mentioned above, which makes it more difficult for the dark states to borrow intensity from the bright one.

Effect of the Number of Monomers. We have computed the excitation energies for the *n*T-C_{60} complexes for n = 2–14 (n even). The geometry of all investigated oligomers shows a very clear bond alternation, which is not affected by the proximity to C_{60} (Figure 7). In the isolated *n*T, each thiophene is twisted by about 150° in relation to the neighboring thiophenes. In the complex with C_{60}, the thiophenes near the fullerene are planarized, while the ones far away remain twisted.

The vertical spectra of the *n*T-C_{60} complexes (n/2 = 1–7) are shown in Figure 8. As expected, the fullerene local states

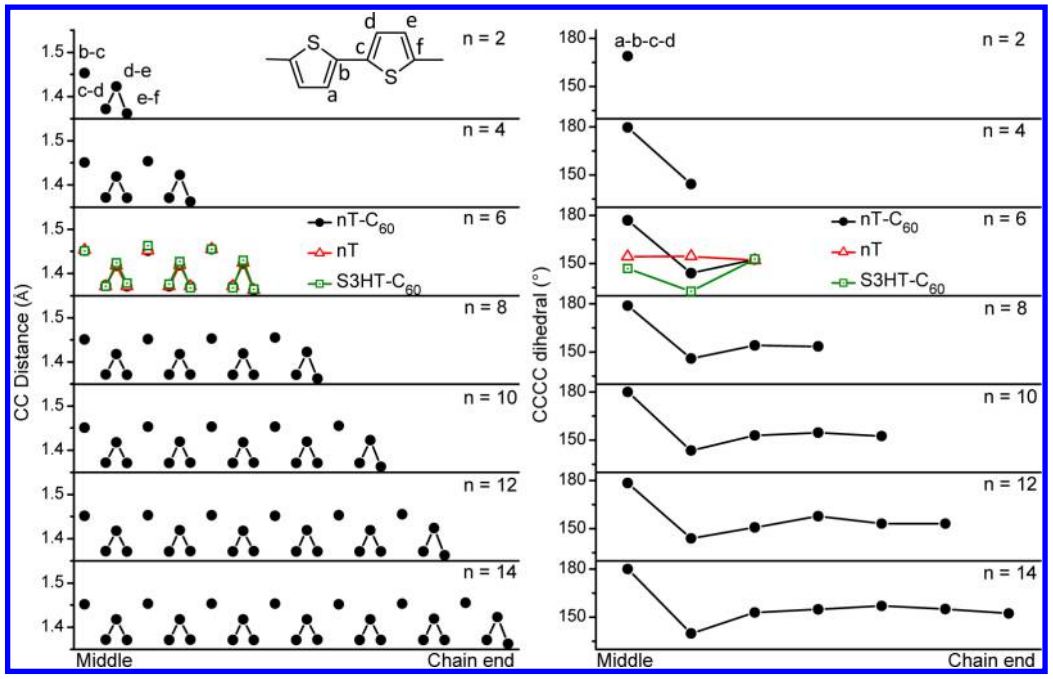

Figure 7. Geometrical parameters for the complexes optimized at the ωB97X-D/6-31G(d) level. All values plotted in this figure are tabulated in the Supporting Information.

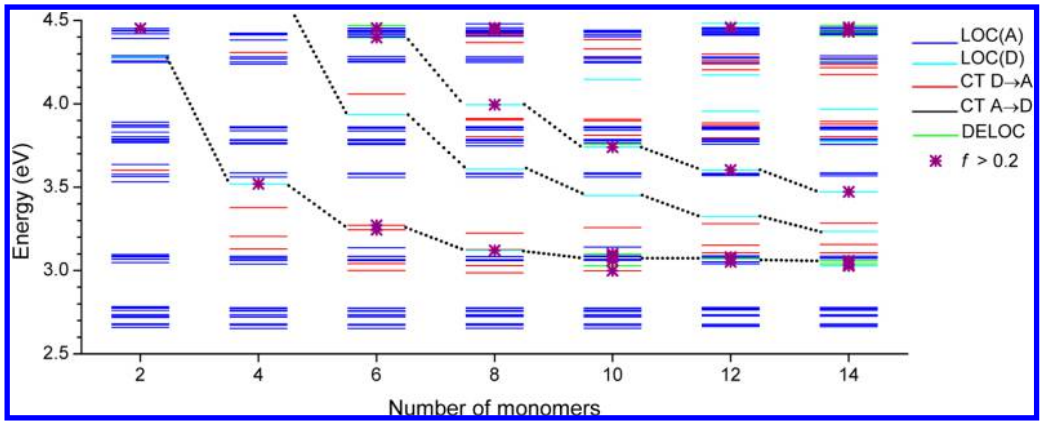

Figure 8. Vertical spectrum of the *n*T-C_{60} ($n/2$ = 1–7) complexes in the gas phase. TD-ωB97X-D/6-31G(d). The dotted lines indicate diabatic connections between selected thiophene states.

[LOC(A)] are not affected by the size of the thiophene chain. The thiophene local states [LOC(D)], on the other hand, are stabilized by the increasing conjugation. The first bright state is 0.2 eV above the asymptotic limit (2.8 eV, see Supporting Information, Table SI-3) for 14T. The asymptotic limit of the experimental band maximum of *n*T is 2.3 eV in benzene[54] and 2.14 eV in dichloromethane and dimethylsulfoxide.[56] The second excited state is stabilized at an even faster rate than the first. The predicted asymptotic limit is also 2.8 eV, indicating that the bands of both states tend to merge for long oligomers. The CT band does not show a strong dependence on the chain length for oligomers with six or more thiophenes. It has a minimum energy for 8T.

Because of the stabilization of the bright states with increasing oligomer size, the first bright state of *n*T starts to mix with the second C_{60} band (1^1H_g state) after connecting 8 monomers. At the asymptotic limit, it should be already on the top of the first C_{60} band. Susceptibility and conductivity measurements of polythiophene film[56] indicate that the effective chain size should contain 9 to 10 monomers (solvated in dimethylsulfoxide, the effective chain is as short as 6 monomers). Therefore, in the film, the first bright state is located very close to the charge transfer states. This means that the excitation of the first bright state may efficiently populate the charge transfer states; however, this should generate cold polarons, which are counterproductive for charge separation.[12]

A series of other interesting features is revealed by Figure 8. First, the bright states are CT states for n = 6 and 10. This apparent contradiction is explained by the multielectronic character of the states: these states receive contributions from configurations with electronic excitation between orbitals localized in different monomers and from configurations with orbitals localized at the same monomer. The first kind contributes to the CT character while the second kind contributes to a large transition dipole moment. One specific example of "bright CT state" is analyzed in detail in section VI of the Supporting Information.

Second, when the stabilization of the bright states with the number of monomers brings these states to the level of the second C_{60} band ($n \geq 8$), some of the states within this band acquire large oscillator strength. This means that states classified as local excitations of C_{60} start to make important contributions to the first bright band. A detailed analysis of such cases (section VII of the Supporting Information) shows that the oscillator strength originates from contributions of thiophene-localized excitations, which are mixed in small amounts into C_{60}-localized states.

Third, the bright states tend to delocalize over the whole complex for chains of 10 or more thiophenes. This opens the possibility of hot-exciton dissociation processes, where charge is separated still in the initially excited state, because of its delocalized character, without populating a CT state. Lee et al.[65] have shown quite convincingly that hot-exciton dissociation should not play a major role in P3HT-PCBM. This means that either delocalization does not take place on P3HT as in nT, or that the hot-exciton dissociation has a small probability of occurrence.

Effect of the D−A Distance. Starting from the ground-state minimum of 6T-C_{60} complex, we have changed the D−A distance keeping all other coordinates at their original values. The upper graph of Figure 9 shows the energies relative to the

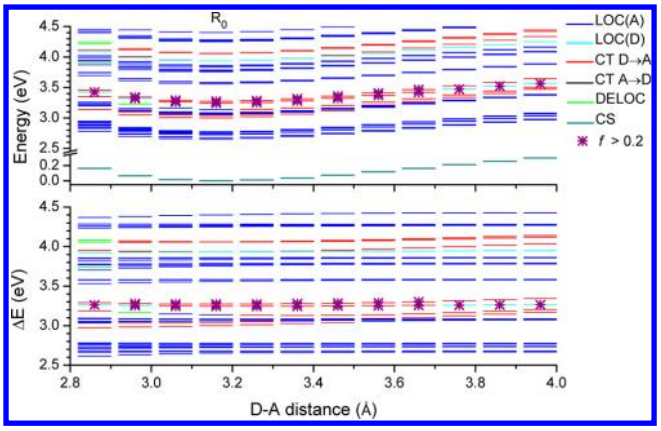

Figure 9. State energies (top) and excitation energies (bottom) of the 6T-C_{60} complex for rigid dissociation along the D−A distance coordinate. TD-ωB97X-D/6-31G(d) results (cs: closed shell). The D−A distance is the shortest C−C distance between 6T and C_{60}.

ground-state minimum of the van-der-Waals well (R_0). The use of dispersion corrections, as included in the ωB97X-D functional, is essential for the proper description of this minimum.

The graph at the bottom of Figure 9 shows the excitation energies along the D−A distance. For each point, the energies are given relative to the ground-state energy computed at the same geometry. These excitation energies show that the CT states are destabilized with increasing distance, as expected. Asymptotically, they show a Coulombic $-q^2/R$ behavior, where q is approximately equal to the transferred charge ΔP_a. The degeneracy of the fullerene bands is broken at short distances, while the local bright states at 6T have constant energy. The amount of charge transfer in the bright state is large enough between 3.1 and 3.7 Å to classify it as CT D→A.

Basis set superposition errors (BSSE) can affect the stabilization of the ground state to a different extent for each D−A distance. This may lead to corrections up to 5 kcal/mol.[66] However, since the excitation energies are computed at a given fixed geometry using the same Kohn−Sham orbitals, the BSSE should be similar for all states, yielding relative energies with a BSSE much smaller than the typical accuracy of the TDDFT energies (around 5 kcal/mol). Therefore, while the state energies shown in Figure 9-top may be affected by BSSE, we do not expect large BSSE effects on the excitation energies in Figure 9-bottom.

Effect of the Environment. The polarizable continuum model (PCM)[67] was used for a simple estimate of the impact of the environment on the excitation energies of the 6T-C_{60} complexes. The dielectric constant was changed between $\varepsilon = 1$ (gas phase) and $\varepsilon = 16$. Thiophene-polymer domains are expected to have $\varepsilon = 3$, while fullerene domains are expected to have $\varepsilon = 4$.[12] Other relevant values are $\varepsilon = 2.3$ for benzene and $\varepsilon = 1.9$ for n-hexane. The results are shown in Figure 10.

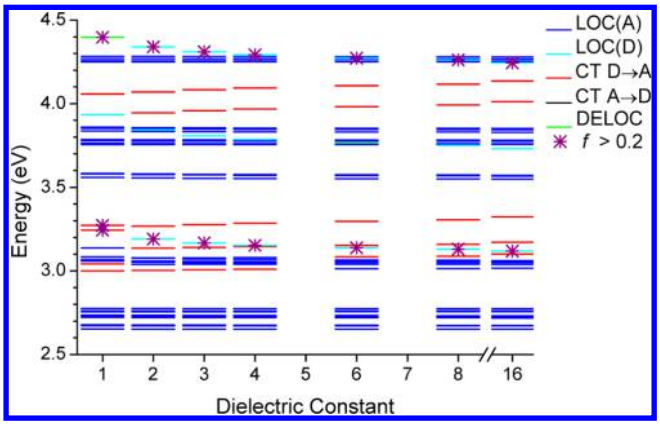

Figure 10. 6T-C_{60} complex with different dielectric constants of a solvation continuum model. TD-ωB97X-D/6-31G(d) + PCM.

Fullerene bands are insensitive to ε. 6T states, however, are slightly stabilized by increasing ε. This stabilization reaches an asymptotic limit at $\varepsilon = 6$, where the bright state is 0.1 eV lower than in the gas phase.

These results indicate that a simple continuum approach cannot fully reproduce the dependence on the environment observed in the experiments. For instance, while the experimental absorption band of C_{60} is shifted by 0.4 eV between an n-hexane solution (3.8 eV, see Table 1)[53] and a solid state film (3.4 eV),[60] the shift in the theoretical PCM result is only 0.05 eV between $\varepsilon = 2$ and $\varepsilon = 4$. In the case of the 6T band, while the experimental shift between 6T in benzene and in solid state is about 0.5−0.6 eV, the theoretical PCM shift is 0.03 eV. The reason for this bad performance is related to two main factors. First, the continuum model does not take into account local electrostatic variations; second, each electronic state may respond differently to the environment depending on the excited state electronic density. Although state-specific continuum models are in principle available,[68] they are too computationally expensive to be employed for tens of states, as required for the description of the D−A heterojunctions. We expect that these problems can be reduced by using hybrid quantum-mechanical/molecular mechanical approaches.[69]

Lessons for a Realistic Heterojunction. We have extended the calculations from the 6T-C_{60} complex to the S3HT-C_{60}, and then to the S3HT-PCBM complex to evaluate the effect of the chemical substitutions on the electronic

spectrum (Figure 11). Because of the large conformational variability of the S3HT oligomer caused by the aliphatic

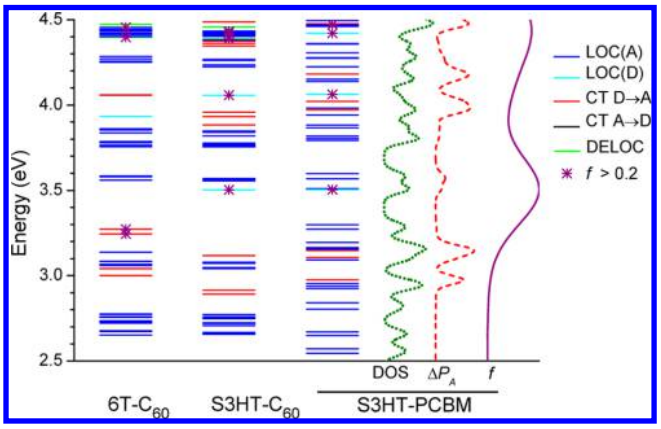

Figure 11. Electronic-state levels of the 6T-C_{60}, S3HT-C_{60}, and S3HT-PCBM complexes. For S3HT-PCBM, convoluted DOS, ΔP_A, and f are shown as well. Calculations at TD-ωB97X-D/6-31G(d) level.

chains,[70] we have decided to work with the *tail-to-tail–head-to-head* (TT-HH) isomer illustrated in Figure 1-c, rather than with the *head-to-tail–head-to-tail* (HT-HT) isomer commonly grown for research on photovoltaics.[71,72] Computationally, the advantage of the former is its rotational symmetry (C_2 point group), which reduces the number of accessible conformations. With the TT-HH isomer, the S3HT-C_{60} complex also has C_2 symmetry and the complex with PCBM is almost symmetric.

The addition of the aliphatic chains to 6T to form S3HT has little effect on C_{60} bands as expected. The local excitations of 6T are, however, destabilized. In particular, the first bright state moves from 3.2 eV in 6T to 3.5 eV in S3HT. This destabilization is a consequence of the lesser conjugation along the oligomer, which is much more twisted in the case of S3HT than in the case of 6T (Figure 7-right). The CT states are only slightly affected, being stabilized by only 0.1 eV. The addition of methyl 5-phenylpentanoate to C_{60} to form PCBM does affect neither the S3HT nor the CT states substantially. Nevertheless, it leads to a spread of the C_{60} states, eliminating large energy gaps and thus increasing the chances of internal conversion.

Strictly from an electronic structure point of view, the S3HT-PCBM complex looks inferior to the 6T-C_{60} complex with regard to its suitability as a photodevice. The blue shift of the bright state and the elimination of the energy gaps in S3HT-PCBM are factors that should tend to reduce charge generation and charge separation, respectively. We note in particular that the CT character of the states at the bottom of the 3 eV band in the 6T-C_{60} complex should be especially favorable to induce charge separation; this feature is lost already in the S3HT-C_{60} complex. In spite of these handicaps, it may turn out that P3HT-PCBM has higher power conversion efficiency than the polyT-C_{60} complex because of other factors beyond the electronic structure. One of them could be that the aliphatic chains extend from the thiophene oligomer to brace the fullerene, which will likely produce a better blend than that with simple thiophene oligomers. Unfortunately, we have not been able to find experimental results obtained under conditions that are similar enough to allow comparing the efficiency of these two complexes and also the occurrence of the blue shift of S3HT-C_{60} in relation to 6T-C_{60}.

On the basis of a single-particle excitation model using Kohn–Sham orbitals (PBE functional), Kanai and Grossman[10] predicted that the lowest excited state of P3HT complexed with C_{60} would be delocalized, enhancing the CT probability. None of our present results using range-separated functionals corroborate this prediction: depending on the chain length, the D–A distance, and the dielectric constant, the lowest CT state may lie in between the first and the second C_{60} bands, but it is always at least 0.2 eV above the lowest excitation.

The reported experimental values for the first band maximum of P3HT-PCBM lie between 2.2 and 3.1 eV (see Table 1). This large range is due to the different fabrication techniques and the varying content of PCBM and P3HT in the film. Values near 2.2 eV are obtained when annealing is employed as deposition technique,[24] suggesting that large domains of pure regioregular P3HT (band maximum at 2.4 eV[23]) are being formed. Values near 3.1 eV are obtained for large amounts of PCBM (>75 wt.%). They are caused by the overlap between the reduced P3HT absorption band and the increasing absorption band of PCBM.[62] The value of 2.6 eV, obtained with spin coating deposition and 50 wt.% PCBM seems to represent a good balance, where the absorption band is disturbed by PCBM, but can still be identified as a P3HT excitation.

As we have discussed, the direct comparison between TDDFT results and the experiments is limited by a series of methodological issues. These limitations are well illustrated by the large difference between the experimental band maximum of P3HT-PCBM, 2.6 eV,[62] and the theoretical vertical excitation energy of S3HT-PCBM, 3.51 eV. We are now in a position to identify the main source of this deviation. First, we have seen that the TDDFT simulated absorption band of 6T is blue-shifted by 0.2 eV compared with the experimental band in benzene. Second, a shift of 0.5 eV is found experimentally between 6T in solution and in the solid state (see Table 1). Third, the extension of the oligomer from 6 monomers to the effective size of 10 monomers is expected to lower the excitation energy by another 0.26 eV (see Figure 8). Taking these factors all together and assuming additivity, we arrive at a corrected theoretical estimate of 3.51 − 0.2 − 0.5 − 0.26 = 2.6 eV, which is in agreement with the experimental value. Naturally, we do not propose that this is the way to proceed to get theoretical predictions. We rather want to point out that the source of deviation between the TDDFT results for a short oligomer in the gas phase and the experimental data for a polymer film can be understood in terms of these three factors. The first one can probably be remedied by the development of new functionals or reparameterization of existing functions targeting specifically large organic complexes. The second and third factors emphasize the need of explicitly including environmental effects, likely via hybrid methods, and the need of considering longer oligomers, respectively.

IV. CONCLUSIONS

The development of organic photovoltaic devices based on donor–acceptor heterojunctions can benefit from computational chemistry. It can help to understand the complex photophysics of these devices and can provide ways to prescreen molecular complexes with high potential for providing efficient devices before synthesis.

The use of computational chemistry in this field has, however, been delayed by the lack of methods allowing accurate predictions of electronically excited states for supra-

molecular systems composed of hundreds of atoms. This situation has started to change with the development of new density functionals that are able to describe charge-transfer states at the TDDFT level. In this article, we have systematically benchmarked TDDFT results for D−A junctions based on thiophene-oligomer/fullerene complexes as a function of several key variables: the density functional, the D−A distance, the number of monomers, the dielectric constant of the environment, and chemical functionalization. These results have been assembled to provide a solid basis for the further development of methodologies that can be used for automatic analysis of D−A heterojunctions in our laboratory, and hopefully by other groups as well.

In addition to the many technical aspects that we have explored, we note some methodological conclusions that have emerged from this work: First, although TDDFT seems to provide a qualitatively adequate description of the electronic structure of D−A heterojunctions, the quantitative results still depend too much on the chosen functional. This naturally implies that more research on density functionals, aiming at a more balanced description of large organic complexes, is needed to enable more reliable computational investigations of organic photovoltaics.

Second, a main source of deviation between the theoretical and experimental results arises from the choice of models containing oligomeric chains that are too short. The experimental results indicate that the polymers effectively behave as long, but finite chains. In the case of thiophene, the effective size is about 10 monomers, which starts to be affordable for localized-basis TDDFT given the current computational capabilities.

Third, the extrapolation of the electronic structure from the gas phase to more realistic solid-state environments is not trivial. According to our present calculations, continuum models seem to be too limited to account for specific environmental effects, leaving as main alternative option the use of hybrid methods with an atomistic description of the environment.

■ ASSOCIATED CONTENT

Ⓢ Supporting Information

Functional characterization, details about state classification and spectrum simulation, asymptotic limits of vertical excitations, collection of experimental data, analysis of CT and C_{60} bright states, geometric parameters, electronic states of the complexes, Cartesian coordinates. This material is available free of charge via the Internet at http://pubs.acs.org.

■ AUTHOR INFORMATION

Corresponding Author

*E-mail: barbatti@kofo.mpg.de.

Notes

The authors declare no competing financial interest.

■ ACKNOWLEDGMENTS

The authors acknowledge fruitful discussions with Dr. J. Götze, Dr. D. Fazzi, Dr. H. Tamura, and Prof. I. Burghardt.

■ REFERENCES

(1) Brédas, J.-L.; Norton, J. E.; Cornil, J.; Coropceanu, V. *Acc. Chem. Res.* **2009**, *42*, 1691−1699.
(2) Deibel, C.; Dyakonov, V. *Rep. Prog. Phys.* **2010**, *73*, 096401.
(3) Clarke, T. M.; Durrant, J. R. *Chem. Rev.* **2010**, *110*, 6736−6767.
(4) Gendron, D.; Leclerc, M. *Energy Environ. Sci.* **2011**, *4*, 1225−1237.
(5) He, F.; Yu, L. *J. Phys. Chem. Lett.* **2011**, *2*, 3102−3113.
(6) Shang, Y.; Li, Q.; Meng, L.; Wang, D.; Shuai, Z. *Theor. Chem. Acc.* **2011**, *129*, 291−301.
(7) Mishra, A.; Bäuerle, P. *Angew. Chem., Int. Ed.* **2012**, *51*, 2020−2067.
(8) Green, M. A.; Emery, K.; Hishikawa, Y.; Warta, W.; Dunlop, E. D. *Prog. Photovoltaics* **2011**, *19*, 565−572.
(9) Bredas, J.; Beljonne, D.; Coropceanu, V.; Cornil, J. *Chem. Rev.* **2004**, *104*, 4971−5003.
(10) Kanai, Y.; Grossman, J. C. *Nano Lett.* **2007**, *7*, 1967−1972.
(11) Cheung, D. L.; McMahon, D. P.; Troisi, A. *J. Am. Chem. Soc.* **2009**, *131*, 11179−11186.
(12) Verlaak, S.; Beljonne, D.; Cheyns, D.; Rolin, C.; Linares, M.; Castet, F.; Cornil, J.; Heremans, P. *Adv. Funct. Mater.* **2009**, *19*, 3809−3814.
(13) Yi, Y.; Coropceanu, V.; Brédas, J.-L. *J. Am. Chem. Soc.* **2009**, *131*, 15777−15783.
(14) Fazzi, D.; Caironi, M.; Castiglioni, C. *J. Am. Chem. Soc.* **2011**, *133*, 19056−19059.
(15) Grancini, G.; Polli, D.; Fazzi, D.; Cabanillas-Gonzalez, J.; Cerullo, G.; Lanzani, G. *J. Phys. Chem. Lett.* **2011**, *2*, 1099−1105.
(16) Isaacs, E. B.; Sharifzadeh, S.; Ma, B.; Neaton, J. B. *J. Phys. Chem. Lett.* **2011**, *2*, 2531−2537.
(17) Lin, L.-Y.; Chen, Y.-H.; Huang, Z.-Y.; Lin, H.-W.; Chou, S.-H.; Lin, F.; Chen, C.-W.; Liu, Y.-H.; Wong, K.-T. *J. Am. Chem. Soc.* **2011**, *133*, 15822−15825.
(18) Minami, T.; Nakano, M.; Castet, F. *J. Phys. Chem. Lett.* **2011**, *2*, 1725−1730.
(19) Tamura, H.; Burghardt, I.; Tsukada, M. *J. Phys. Chem. C* **2011**, *115*, 10205−10210.
(20) Baumeier, B.; Andrienko, D.; Rohlfing, M. *J. Chem. Theory Comput.* **2012**, *8*, 2790−2795.
(21) Fazzi, D.; Grancini, G.; Maiuri, M.; Brida, D.; Cerullo, G.; Lanzani, G. *Phys. Chem. Chem. Phys.* **2012**, *14*, 6367−6374.
(22) Petrozza, A.; Fazzi, D.; Avilov, I.; Beljonne, D.; Friend, R. H.; Kim, J.-S. *J. Phys. Chem. C* **2012**, *116*, 11298−11305.
(23) Brown, P. J.; Thomas, D. S.; Köhler, A.; Wilson, J. S.; Kim, J.-S.; Ramsdale, C. M.; Sirringhaus, H.; Friend, R. H. *Phys. Rev. B* **2003**, *67*, 064203.
(24) Faist, M. A.; Keivanidis, P. E.; Foster, S.; Wöbkenberg, P. H.; Anthopoulos, T. D.; Bradley, D. D. C.; Durrant, J. R.; Nelson, J. *J. Polym. Sci., Part B: Polym. Phys.* **2011**, *49*, 45−51.
(25) Chai, J.-D.; Head-Gordon, M. *Phys. Chem. Chem. Phys.* **2008**, *10*, 6615−6620.
(26) Becke, A. D. *J. Chem. Phys.* **1993**, *98*, 5648−5652.
(27) Stephens, P. J.; Devlin, F. J.; Chabalowski, C. F.; Frisch, M. J. *J. Phys. Chem.* **1994**, *98*, 11623−11627.
(28) Perdew, J. P.; Burke, K.; Ernzerhof, M. *Phys. Rev. Lett.* **1996**, *77*, 3865−3868.
(29) Iikura, H.; Tsuneda, T.; Yanai, T.; Hirao, K. *J. Chem. Phys.* **2001**, *115*, 3540−3544.
(30) Becke, A. D. *Phys. Rev. A* **1988**, *38*, 3098−3100.
(31) Lee, C.; Yang, W.; Parr, R. G. *Phys. Rev. B* **1988**, *37*, 785−789.
(32) Yanai, T.; Tew, D. P.; Handy, N. C. *Chem. Phys. Lett.* **2004**, *393*, 51−57.
(33) Zhao, Y.; Truhlar, D. *Theor. Chem. Acc.* **2008**, *119*, 525−525.
(34) Zhao, Y.; Truhlar, D. G. *J. Phys. Chem. A* **2006**, *110*, 13126−13130.
(35) Hehre, W. J.; Ditchfield., R.; Pople, J. A. *J. Chem. Phys.* **1972**, *56*, 2257−2261.
(36) Frisch, M. J.; Trucks, G. W.; Schlegel, H. B.; Scuseria, G. E.; Robb, M. A.; Cheeseman, J. R.; Scalmani, G.; Barone, V.; Mennucci, B.; Petersson, G. A.; Nakatsuji, H.; Caricato, M.; Li, X.; Hratchian, H. P.; Izmaylov, A. F.; Bloino, J.; Zheng, G.; Sonnenberg, J. L.; Hada, M.; Ehara, M.; Toyota, K.; Fukuda, R.; Hasegawa, J.; Ishida, M.; Nakajima, T.; Honda, Y.; Kitao, O.; Nakai, H.; Vreven, T.; Montgomery, J., J. A.; Peralta, J. E.; Ogliaro, F.; Bearpark, M.; Heyd, J. J.; Brothers, E.; Kudin,

K. N.; Staroverov, V. N.; Kobayashi, R.; Normand, J.; Raghavachari, K.; Rendell, A.; Burant, J. C.; Iyengar, S. S.; Tomasi, J.; Cossi, M.; Rega, N.; Millam, N. J.; Klene, M.; Knox, J. E.; Cross, J. B.; Bakken, V.; Adamo, C.; Jaramillo, J.; Gomperts, R.; Stratmann, R. E.; Yazyev, O.; Austin, A. J.; Cammi, R.; Pomelli, C.; Ochterski, J. W.; Martin, R. L.; Morokuma, K.; Zakrzewski, V. G.; Voth, G. A.; Salvador, P.; Dannenberg, J. J.; Dapprich, S.; Daniels, A. D.; Farkas, Ö.; Foresman, J. B.; Ortiz, J. V.; Cioslowski, J.; Fox, D. J. *Gaussian 09*, Revision A.02; Gaussian, Inc.: Wallingford, CT, 2009.

(37) Crespo-Otero, R.; Barbatti, M. *Theor. Chem. Acc.* **2012**, *131*, 1237.

(38) Casida, M. Time-dependent density functional response theory for molecules. In *Recent advances in density functional methods, Part I*; Chong, D., Ed.; World Scientific: Singapore, 1995; pp 155−192.

(39) Barbatti, M.; Aquino, A. J. A.; Lischka, H. *Phys. Chem. Chem. Phys.* **2010**, *12*, 4959−4967.

(40) Barbatti, M.; Granucci, G.; Persico, M.; Ruckenbauer, M.; Vazdar, M.; Eckert-Maksić, M.; Lischka, H. *J. Photochem. Photobiol., A* **2007**, *190*, 228−240.

(41) Barbatti, M.; Granucci, G.; Ruckenbauer, M.; Plasser, F.; Pittner, J.; Persico, M.; Lischka, H. *NEWTON-X: a package for Newtonian dynamics close to the crossing seam*; 2012; www.newtonx.org.

(42) Grimme, S.; Waletzke, M. *J. Chem. Phys.* **1999**, *111*, 5645−5655.

(43) Ahlrichs, R.; Bär, M.; Häser, M.; Horn, H.; Kölmel, C. *Chem. Phys. Lett.* **1989**, *162*, 165−169.

(44) Becke, A. D. *J. Chem. Phys.* **1993**, *98*, 1372−1377.

(45) Weigend, F.; Ahlrichs, R. *Phys. Chem. Chem. Phys.* **2005**, *7*, 3297−3305.

(46) Weigend, F.; Häser, M.; Patzelt, H.; Ahlrichs, R. *Chem. Phys. Lett.* **1998**, *294*, 143−152.

(47) Dreuw, A.; Head-Gordon, M. *Chem. Rev.* **2005**, *105*, 4009−4037.

(48) Wong, B. M.; Hsieh, T. H. *J. Chem. Theory Comput.* **2010**, *6*, 3704−3712.

(49) Gordon, M. S.; Schmidt, M. W. Advances in electronic structure theory: GAMESS a decade later. In *Theory and Applications of Computational Chemistry the first forty years*; Dykstra, C. E., Frenking, G., Kim, K. S., Scuseria, G. E., Eds.; Elsevier: Amsterdam, The Netherlands, 2005; pp 1167−1189.

(50) Tawada, Y.; Tsuneda, T.; Yanagisawa, S.; Yanai, T.; Hirao, K. *J. Chem. Phys.* **2004**, *120*, 8425−8433.

(51) Silva-Junior, M. R.; Schreiber, M.; Sauer, S. P. A.; Thiel, W. *J. Chem. Phys.* **2008**, *129*, 104103.

(52) Maitra, N. T.; Zhang, F.; Cave, R. J.; Burke, K. *J. Chem. Phys.* **2004**, *120*, 5932−5937.

(53) Leach, S.; Vervloet, M.; Desprès, A.; Bréheret, E.; Hare, J. P.; John Dennis, T.; Kroto, H. W.; Taylor, R.; Walton, D. R. M. *Chem. Phys.* **1992**, *160*, 451−466.

(54) de Melo, J. S.; Burrows, H. D.; Svensson, M.; Andersson, M. R.; Monkman, A. P. *J. Chem. Phys.* **2003**, *118*, 1550−1556.

(55) Heller, E. J. *Acc. Chem. Res.* **1981**, *14*, 368−375.

(56) Sears, W. M.; MacKinnon, C. D.; Kraft, T. M. *Synth. Met.* **2011**, *161*, 1566−1574.

(57) Sakai, J.; Taima, T.; Saito, K. *Org. Electron.* **2008**, *9*, 582−590.

(58) Kouki, F.; Spearman, P.; Valat, P.; Horowitz, G.; Garnier, F. *J. Chem. Phys.* **2000**, *113*, 385−391.

(59) Orlandi, G.; Negri, F. *Photochem. Photobiol. Sci.* **2002**, *1*, 289−308.

(60) Schwedhelm, R.; Kipp, L.; Dallmeyer, A.; Skibowski, M. *Phys. Rev. B* **1998**, *58*, 13176−13180.

(61) Kobayashi, T.; Kinoshita, K.; Nagase, T.; Naito, H. *Phys. Rev. B* **2011**, *83*, 035305.

(62) Shrotriya, V.; Ouyang, J.; Tseng, R. J.; Li, G.; Yang, Y. *Chem. Phys. Lett.* **2005**, *411*, 138−143.

(63) Bauernschmitt, R.; Ahlrichs, R.; Hennrich, F. H.; Kappes, M. M. *J. Am. Chem. Soc.* **1998**, *120*, 5052−5059.

(64) Montero-Alejo, A. L.; Menendez-Proupin, E.; Fuentes, M. E.; Delgado, A.; Montforts, F. P.; Montero-Cabrera, L. A.; Garcia de la Vega, J. M. *Phys. Chem. Chem. Phys.* **2012**, *14*, 13058−13066.

(65) Lee, J.; Vandewal, K.; Yost, S. R.; Bahlke, M. E.; Goris, L.; Baldo, M. A.; Manca, J. V.; Voorhis, T. V. *J. Am. Chem. Soc.* **2010**, *132*, 11878−11880.

(66) Isla, H.; Grimm, B.; Perez, E. M.; Rosario Torres, M.; Angeles Herranz, M.; Viruela, R.; Arago, J.; Orti, E.; M. Guldi, D.; Martin, N. *Chem. Sci.* **2012**, *3*, 498−508.

(67) Tomasi, J.; Mennucci, B.; Cammi, R. *Chem. Rev.* **2005**, *105*, 2999−3094.

(68) Improta, R.; Barone, V.; Scalmani, G.; Frisch, M. J. *J. Chem. Phys.* **2006**, *125*, 054103−054109.

(69) Senn, H. M.; Thiel, W. *Angew. Chem., Int. Ed.* **2009**, *48*, 1198−1229.

(70) Liu, T.; Cheung, D. L.; Troisi, A. *Phys. Chem. Chem. Phys.* **2011**, *13*, 21461−21470.

(71) McCullough, R. D. *Adv. Mater.* **1998**, *10*, 93−116.

(72) Hugger, S.; Thomann, R.; Heinzel, T.; Thurn-Albrecht, T. *Colloid Polym. Sci.* **2004**, *282*, 932−938.